HIGH-RESOLUTION MICROSTRUCTURAL ANALYSIS OF SHOCK DEFORMATION IN APATITE FROM THE CHICXULUB IMPACT STRUCTURE. Morgan A. Cox[1,2], Timmons M. Erickson[1,3], Martin Schmieder[2], Roy Christoffersen[3], Daniel K. Ross[3], Aaron J. Cavosie[1], Phil A. Bland[1], and David A. Kring[2]. [1]Space Science and Technology Centre (SSTC), School of Earth and Planetary Science, Curtin University, Perth, WA 6102, Australia. [2]Lunar and Planetary Institute (LPI) – USRA, 3600 Bay Area Boulevard, Houston, TX 77058, USA [3]Jacobs - JETS, Astromaterials Research and Exploration Science Division, NASA Johnson Space Center, Houston, Texas, 77058, USA. (Email: morgan.cox@student.curtin.edu.au)

Introduction: The phosphate apatite, $Ca_5(PO_4)_3(F,Cl,OH)$, is a ubiquitous accessory mineral found in both terrestrial and extraterrestrial rocks. It is commonly used to study planetary volatile abundances and, because it is a U–Pb carrier, to determine the ages of geologic events (e.g., [1]). The utility of apatite may be affected by impact cratering processes that produce shock-deformation microstructures within the mineral, including planar fractures, partial to full-scale recrystallization, and low angle grain boundaries, which have been observed in both terrestrial and extraterrestrial samples [2-6]. To better ascertain what type of deformation occurs during hyper-velocity impacts we conducted a detailed microstructural analysis of crystals in ~550 m of shocked granitoid rocks and impact melt rocks in a core from the peak ring of the Chicxulub impact structure (Fig. 1).

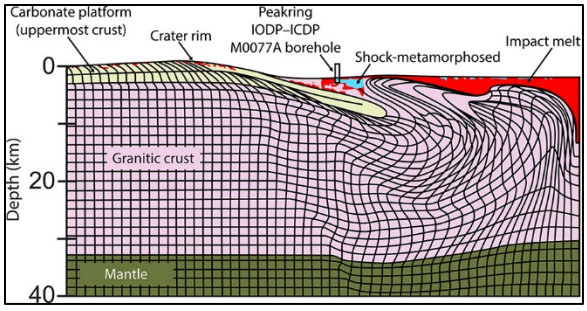

Figure 1. *Location of core recovered by IODP-ICDP Expedition 364 to the Chicxulub impact crater. Illustration from [7].*

Samples and Methods: Seventeen samples from core M0077A into the Chicxulub peak ring [8] were selected representing the interval 745 to 1320 meters below sea floor. A total of 560 apatite crystals were identified and imaged using optical microscopy and back-scattered electron. Microstructural analyses of a subset of 108 apatite crystals were made with an Oxford Symmetry electron backscatter diffraction (EBSD) detector on a JEOL 7600f field emission gun SEM at JSC. Acquisition parameters included a 20 kV accelerating voltage, 18 nA beam current, 20.5 mm working distance, and 70° sample tilt. Step sizes of EBSD maps were between 700 and 50 nm.

A focused ion beam foil (FIB) was prepared perpendicular to a systematic planar deformation band identified within one of the apatite grains. The FIB foil was then analyzed using transmission Kikuchi diffraction (TKD) mapping and transmission electron microscopy (TEM) in order to characterize the planar deformation bands in detail.

Electron microprobe analysis was then conducted on a subset of apatite grains from impact melt rock and impact melt veins in order to determine any changes in chemistry (e.g., comparing weakly deformed with shock-recrystallized grains) which may have resulted from the impact event.

Results: Apatite crystals range in length from 30 to 900 µm and exhibit euhedral to subhedral basal and prism crystal structures. Optical imaging of apatite crystals revealed planar fractures (PFs), sub-planar fractures, cataclastic deformation, and granular textures. A total of ~250 apatite crystals contain PFs. Up to three orientations of PFs were identified within a single apatite crystal. Planar fractures within the apatite crystals form conjugate sets that are oriented within either $\{\bar{2}110\}$, $\{2\bar{1}\bar{1}0\}$, $\{\bar{1}\bar{1}20\}$, or $\{11\bar{2}0\}$. Offsets along planar fractures are also identified in heavily fractured crystals, with up to ~5 µm of apparent displacement. Sub-planar fractures are common within apatite. Cataclastic deformation is observed in 60 crystals. Some crystals are sheared along fractures.

Seven apatite crystals within impact melt rock (sample 728.515 mbs) and melt veins and (sample 917.295 mbsf) contain granular microstructures. Crystals are ~10 to 100 µm in size and contain a mixture of rounded neoblastic microstructures and larger euhedral laths.

Electron backscatter diffraction analyses of 108 apatite crystals from granitoid and impact melt rock indicate plastic deformation affected apatite throughout the core. Crystals containing planar fractures (PFs) exhibit a higher degree of apparent deformation. Planar deformation bands (PDBs) are observed in 5 crystals, with PDBs systematically misorientated up to 20˚ from the host in preferred crystallographic orientations (Fig. 1). Crystallographically-controlled planar deformation bands are consistent with tilt boundaries that contain <c> and result from slip in $<10\bar{1}0>$ on $\{\bar{1}\bar{1}20\}$ during

shock deformation (Fig. 2). Cataclastically deformed crystals exhibit >40˚ of misorientation of rotated fragments, with surrounding quartz showing a high degree of crystal-plastic deformation as well.

High-resolution EBSD mapping of partially re-crystallized grains from the impact melt unit shows that host apatite crystals contain large dispersions in pole figures due to impact-induced deformation, while newly recrystallized domains show little to no dispersion on pole figures indicating that they are strain-free domains. Fully recrystallized grains show differences in crystallinity, with one grain containing a newly re-crystallized rim of apatite, while the interior of the crystal does not map by EBSD. Apatite included in sheet silicates show very low levels of crystal-plastic deformation, with <5˚ of misorientation observed, while crystals in contact with zircon and/or quartz show up to 20˚ of misorientation across the crystal, with a high degree of deformation at the contact between apatite and zircon or quartz.

The FIB foil of a planar deformation band within apatite analyzed through TKD shows that the deformation band has little dispersion around the c-axis, while the other main axes are largely dispersed (Fig. 2). Transmission electron microcopy analysis of the FIB foil shows that the PDB boundaries are made up of complex dislocation networks. Bright-field STEM imaging of the c-axis orientation of the crystal shows near-extinction of dislocations that define the deformation band, suggesting that the Burgers vector b of the dislocations have a significant c-axis component or are completely parallel to <0001>.

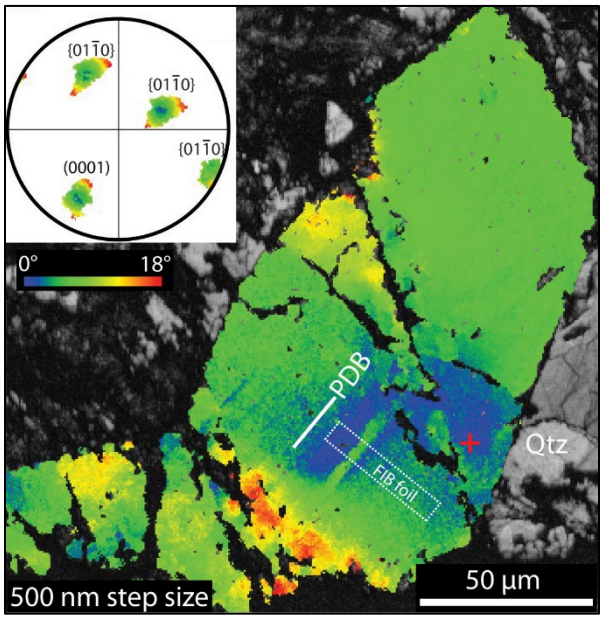

Figure 2*. Texture component map showing mis-orientation within apatite grain in shocked granitoid. Grain has PDBs that are up to 18° misoriented from the host grain. 168-3-25-27 (932.79 mbsf).*

Electron microprobe analysis shows that apatite crystals from the uppermost impact melt rock are chlorine rich (~0.3 to 0.8 wt.%), while crystals from impact melt veins lower in the core have less Cl (<0.1 wt.%). All apatite crystals are fluorine rich with F concentrations ranging from ~3 to ~4 wt% within the samples investigated. The partially recrystallized grain shows that in recrystallized domains there is higher Mg, with concentrations ranging from ~0.01 to 0.2 wt.% MgO, while Mg in pre-existing apatite crystal is typically the microprobe below detection limit.

Conclusions: The inferred change in chemistry of apatite coupled with the development of shock microstructures highlights the need to utilize multiple techniques when characterizing apatite crystals that have experienced high pressures and temperatures during one or more hyper-velocity impact events. By using multiple techniques, we are able to develop a better understanding of how the mineral responds to shock deformation.

Acknowledgement: This study was conducted in the 2019 edition of the LPI Summer Intern Program in Planetary Science. We thank the scientists of IODP-ICDP Expedition 364 for recovering and logging the core.

References: [1] Chew D. M. and Spikings R. A. (2015) *Elements 11*, 189–194. [2] Cavosie A. J. and Lugo Centeno C. (2014) *LPS XLV, Abstract #1691*. [3] McGregor M. et al. (2018) *Earth Planet. Sci. Lett., 504*, 185–197. [4] Černok A. et al. (2019) *Meteoritics & Planet. Sci,, 54*, 1262–1282. [5] Kenny G. et al. (2020) *Geology, 48*, 19–23. [6] Shaulis B. J. et al. (2016) *LPS XLVII*, Abstract #2027. [7] Kring D. A. et al. (2017) *GSA Today 27(10)*, 4–8. [8] Morgan et al., 2016, Science.